BIOCHEMISTRY
including biophysical chemistry & molecular biology

Article

pubs.acs.org/biochemistry

Exploring the Catalytic Mechanism of Human Glutamine Synthetase by Computer Simulations

Federico M. Issoglio,[†] Nicolas Campolo,[‡,§] Ari Zeida,[†] Tilman Grune,[⊥] Rafael Radi,[‡,§] Dario A. Estrin,*[,†] and Silvina Bartesaghi*[,‡,§,∥]

[†]Departamento de Química Inorgánica, Analítica y Química-Física and INQUIMAE-CONICET, Facultad de Ciencias Exactas y Naturales, Universidad de Buenos Aires, Buenos Aires, Argentina

[‡]Departamento de Bioquímica and [§]Center for Free Radical and Biomedical Research, Facultad de Medicina, Universidad de la República, Montevideo, Uruguay

[∥]Departamento de Educación Médica, Facultad de Medicina, Universidad de la República, Montevideo, Uruguay

[⊥]German Institute of Human Nutrition (DIfE) Potsdam-Rehbrücke, Department of Molecular Toxicology, Arthur-Scheunert-Allee 114-116, 14558 Nuthetal, Germany

Supporting Information

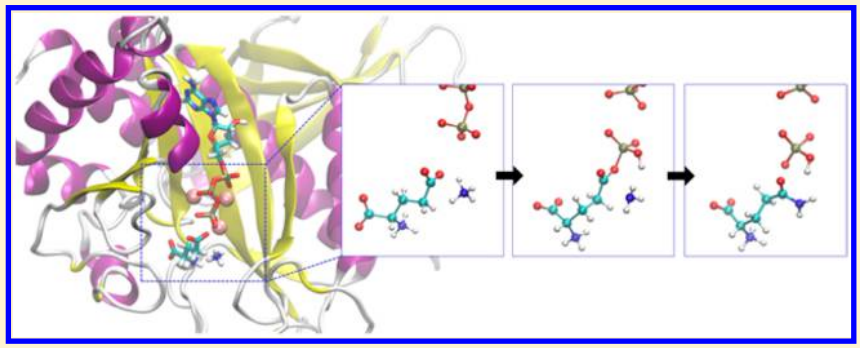

ABSTRACT: Glutamine synthetase is an important enzyme that catalyzes the ATP-dependent formation of glutamine from glutamate and ammonia. In mammals, it plays a key role in preventing excitotoxicity in the brain and detoxifying ammonia in the liver. In plants and bacteria, it is fundamental for nitrogen metabolism, being critical for the survival of the organism. In this work, we show how the use of classical molecular dynamics simulations and multiscale quantum mechanics/molecular mechanics simulations allowed us to examine the structural properties and dynamics of human glutamine synthetase (*Hs*GS), as well as the reaction mechanisms involved in the catalytic process with atomic level detail. Our results suggest that glutamine formation proceeds through a two-step mechanism that includes a first step in which the γ-glutamyl phosphate intermediate forms, with a 5 kcal/mol free energy barrier and a −8 kcal/mol reaction free energy, and then a second rate-limiting step involving the ammonia nucleophilic attack, with a free energy barrier of 19 kcal/mol and a reaction free energy of almost zero. A detailed analysis of structural features within each step exposed the relevance of the acid−base equilibrium related to protein residues and substrates in the thermodynamics and kinetics of the reactions. These results provide a comprehensive study of *Hs*GS dynamics and establish the groundwork for further analysis regarding changes in *Hs*GS activity, as occur in natural variants and post-translational modifications.

Glutamine synthetase (GS) is an essential enzyme in nitrogen metabolism that catalyzes the ATP-dependent synthesis of glutamine from glutamate and ammonia using ATP and Mg^{2+} or Mn^{2+} as cofactors (Scheme 1), assimilating thus inorganic nitrogen into an organic intermediate that can act as a main source of nitrogen for the synthesis of amino acids and nucleotides. Because of this critical role, GS enzymes are ubiquitous and well-conserved among all life domains, from primitive unicellular organisms to higher vertebrates, and they are thought to be some of the oldest functioning enzymes.[1−3]

On the basis of sequence, structure, and certain functional aspects, three types of glutamine synthetases have been described in the GS family: GSI, the main form present in prokaryotes, GSII, mostly found in eukaryotes, and GSIII, the most recently recognized one, which is found in only certain prokaryotes. Despite this generality, there are some prokaryotes that also possess GSII, and GSI genes have also been found on eukaryotes, a fact that is consistent with the hypothesis that these two types of GS were produced by gene duplication more than 1000 million years before the divergence between prokaryotes and eukaryotes occurred.[3−7]

Received: August 9, 2016
Revised: September 27, 2016
Published: September 29, 2016

DOI: 10.1021/acs.biochem.6b00822
Biochemistry 2016, 55, 5907−5916

Scheme 1. Reaction Catalyzed by GS

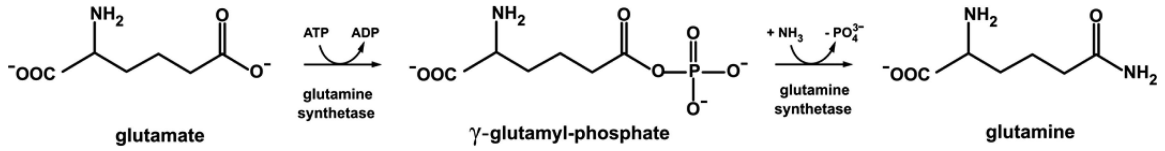

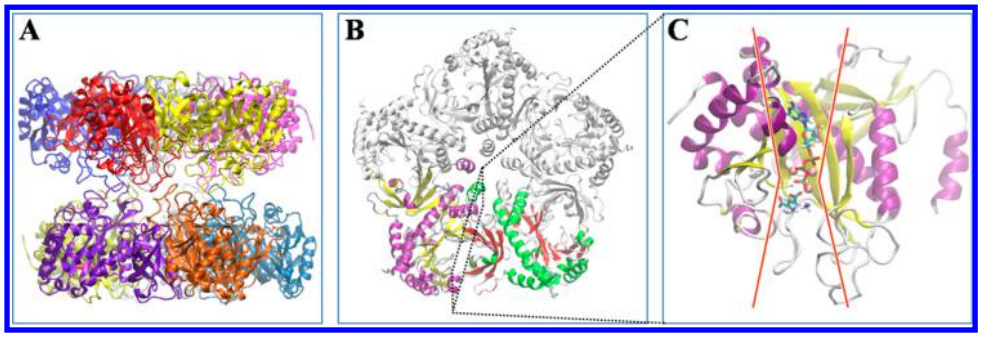

Figure 1. (A) *Hs*GS decamer represented as ribbons and colored by subunit. (B) Pentameric ring represented with ribbons. Only two subunits were colored according to their secondary structure (one subunit in purple and yellow and the other in green and red for α-helices and β-sheets, respectively). (C) The active site has a double-funnel shape, with three binding sites for Mn^{2+} or Mg^{2+} located at the center. ATP, glutamate, and ammonium are illustrated in "licorice" representation and colored by atom type. Only one subunit involved in the active site is depicted for the sake of clarity.

To date, the three-dimensional structure members of the three types of GS is known.[1,8−10] They are all large homo-oligomeric proteins composed of two closed ring structures that associate across an interface and are arranged with dihedral symmetry.[1] In all cases, the active sites are located at the interface between two monomers at each ring;[9] the active site has a bifunnel shape and contains three divalent cation binding sites that are occupied by manganese or magnesium ions.[11] Type I GS and type III GS are all dodecameric oligomers formed from two hexameric rings of subunits, with 12 active sites located between the monomers.[11] Type II GSs are similarly arranged but are decameric oligomers, formed by the interaction of two pentameric rings, having therefore 10 active sites per enzyme molecule. Human glutamine synthetase (*Hs*GS) is an example of GSII constituted by 42 kDa monomers of 373 amino acids that are arranged as described previously (Figure 1).[8,9]

In microorganisms and plants, GS plays its major roles in the assimilation and recycling of nitrogen. Plants and certain animals express different isoforms of type II GS, presenting different subcellular localizations (cytosol and chloroplasts or mitochondria) and distinct patterns of expression in different tissues.[4,12−14] In most vertebrates, however, a single GS isoform is expressed, although it also presents a cytosolic and mitochondrial distribution and tissue-specific expression. In this case, the alternative splicing of the single GS gene is responsible for the differential expression of GS in vertebrate organisms.[15] Although in animals GS also plays an important role in nitrogen metabolism by producing glutamine, it has adapted to play other specific roles. Given the high toxicity of ammonia to animals, in these organisms, GS acts as an important pathway for ammonia detoxification. Most of this function is achieved by hepatic GS (where it has a mitochondrial location) and is one of the major tissues in which it is expressed in vertebrates. The other major site of expression is the brain (mainly at the cytosol of astrocytes), where, besides detoxifying ammonia, it has a key function in sustaining the glutamate−glutamine cycle, removing excess neurotransmitter glutamate, and preventing glutamate excitotoxicity.[9,16,17] Because of its key role in maintaining brain homeostasis, changes in the levels or activity of glutamine synthetase may result in astroglial dysfunction, affecting severely neuronal survival.[18] Indeed, the loss of GS activity has been related to neurodegenerative disorders, such as Alzheimer's disease, both in animal models and in human patients.[19−21] Furthermore, several studies have observed a decrease in GS activity with aging.[22,23] In addition, under inflammatory and/or oxidative stress conditions, mammalian GS may be oxidatively modified (e.g., tyrosine-nitrated), leading to a loss of activity *in vivo*. The critical role of GS becomes evident when rare clinical cases of punctual mutations on GS identified in human patients are considered, which were connected to congenital glutamine deficiency with severe brain malformation, resulting in multiorgan failure and neonatal death.[24,25]

Initial biochemical and enzymological studies characterized the reaction catalyzed by GS, suggesting the two-step model for glutamine biosynthesis accepted today, that implies the initial formation of the activated intermediate γ-glutamyl phosphate (γ-Glu-P), followed by the nucleophilic attack of ammonia on that intermediate, releasing phosphate and yielding glutamine.[11,26−28] Crystal structures of different enzyme−substrate complexes led to the proposal of a structural model for the reaction mechanism of GSI, defining the role of several active site amino acids in catalysis.[29] However, to date, there are no accurate studies related to the active site structural features that are the molecular determinants of catalytic activity, especially for type II GS. A structural analysis of *Hs*GS that includes the use of molecular dynamics (MD) simulations to describe the impact of single-residue mutations on the structural dynamics of three inactive enzymes bearing a natural variation has been reported,[30] and very recently, Moreira et al. published a computational study of the reaction mechanism of *Mycobacterium tuberculosis* GS.[31] Despite this, no detailed analysis regarding *Hs*GS reaction mechanisms involved in the catalysis of glutamine formation from glutamate and ammonia with

DOI: 10.1021/acs.biochem.6b00822
Biochemistry 2016, 55, 5907−5916

atomic level resolution has been published. Our work includes a quantum treatment of the active site immersed in a classical description of the rest of the system [quantum mechanics/molecular mechanics (QM/MM)] that allowed us to examine the chemical reactivity. We employed multiple steered molecular dynamic (MSMD) simulations to construct the free energy profiles for each reaction catalyzed by *Hs*GS. The studies reported herein help to rationalize the mechanism of action of GS with an atomic level of detail.

METHODS

Molecular Dynamics Simulations. A pK_a prediction of ionizable protein residues was made with PROPKA,[32] using the crystallographic structure from which all the systems studied were constructed (see below). Considering the PROPKA-computed values and via examination of the crystal structure with Visual Molecular Dynamics (VMD),[33] protonation states were assigned for titratable residues, promoting hydrogen bond formation. Only residue E305 showed a pK_a value that required further attention (~7.8 on average according to the PROPKA calculation). Moreover, the E305 carboxyl oxygen has a distance of ~2.5 Å to the carboxyl oxygen of the D62 residue from the adjacent subunit (D62′ hereafter). All these together suggest that a strong hydrogen bond interaction may be present between these two residues. MD simulations for wild-type *Hs*GS were performed under seven different conditions (see Table 1). First, we considered the conditions for each step of the reaction, e.g., the enzyme complexed with the initial reactants for the first step, and with all possible combinations of intermediate and substrates for the second step of the reaction. Also, all the systems were analyzed taking into account residue E305 in its two protonation states, as glutamate and as glutamic acid.

Table 1. List of MD Simulations Performed in This Study[a]

simulation	reactants			
1	ATP	Glu	–	E305-COO^-
2	ATP	Glu	–	E305-COOH
3	ADP	γ-Glu-P	NH_3	E305-COO^-
4	ADP	γ-Glu-P	NH_3	E305-COOH
5	ADP	γ-Glu-P	NH_4^+	E305-COO^-
6	ADP	γ-Glu-P	NH_4^+	E305-COOH
7	ADP	γ-Glu−P-H	NH_3	E305-COOH

[a]Simulations 1 and 2 correspond to reactants for the first step, and simulations 3−7 include the possible reactants for the second step of the reaction mechanism.

To build these systems, we used atomic coordinates from the crystal structure complexed with ADP, manganese ions (Mn^{2+}), and the inhibitor L-methionine-*S*-sulfoximine phosphate (MSO-P) determined at 2.6 Å resolution[9] [Protein Data Bank (PDB) entry 2QC8]. The determined structure also shows chloride ions (one for each subunit) and crystallographic water molecules that were kept for the startup structure. ATP, glutamate, and γ-Glu-P were constructed manually from the coordinates of ADP and MSO-P. NH_3 and NH_4^+ were placed using the coordinates of the methyl group of the MSO-P, proposed to be positioned at or near the ammonium binding site.[9] Parameters for zwitterionic glutamate and γ-glutamyl phosphate (protonated on the phosphate moiety or not), NH_3, and NH_4^+ were obtained from an electronic structure calculation using Gaussian03 at the HF/6-31G* level basis set, followed by a derivation of partial atomic charges using the RESP procedure.[34] Force field parameters and partial charges for the polyphosphate chains of ADP and ATP were taken from ref 35. The AMBER14SB force field was chosen to assign parameters of all protein residues. The pentamer of *Hs*GS was used for MD, which allowed us to reduce the high computational cost associated with the decamer yet provided results by quintuplicate for statistical analysis. In each case, the system was placed into a truncated octahedral box of TIP3P water molecules, defining a distance of 15 Å between the border of the box and the closest atom of the solute. This gave us a total of ~190000 atoms in the system, with ~54000 water molecules and 1779 protein residues. All the systems were optimized with two steps of energy minimization, each consisting of 400 cycles with a 500 kcal mol^{-1} $Å^{-2}$ force constant applied over all atoms excluding water molecules in the former and over backbone atoms only in the latter. The temperature was increased from 0 to 10 K in a 10 ps constant volume MD with a 0.1 fs time step, and a harmonic restraint potential of 50 kcal mol^{-1} $Å^{-2}$ applied over all protein residues, ions, ligands, and water molecules involved in the coordination of Mn^{2+}. Thereafter, the temperature was increased from 10 to 300 K in a 90 ps constant volume MD with a 0.5 fs time step, applying a force constant of 10 kcal mol^{-1} $Å^{-2}$ to the protein backbone atoms, ions, ligands, and water molecules involved in the coordination of Mn^{2+}. After the samples had been heated, the density was equilibrated with a 400 ps MD simulation at constant temperature and pressure with a time step of 1 ps, and applying a force constant of 1 kcal mol^{-1} $Å^{-2}$ to the protein backbone atoms, ions, ligands, and water molecules involved in the coordination of Mn^{2+}. To control temperature, a Langevin thermostat was used, whereas a Berendsen barostat was chosen to adjust the pressure to 1 bar (both regulated every 1 ps). For production MD, 100 ns simulations in the *NTP* ensemble were conducted, with a time step of 2 fs. All the simulations were performed under periodic boundary conditions[36] using the SHAKE algorithm[37] to keep hydrogen atoms at equilibrium bond lengths. Long range electrostatic interactions were handled with Ewald sums, setting a cutoff distance of 10 Å.

Implicit Ligand Sampling. Migration of ammonia inside the *Hs*GS environment was analyzed with an implicit ligand sampling (ILS) approach,[38,39] to explore the tunnels and cavities through which this ligand is capable of reaching the active site. Calculations were performed over 1000 representative frames equally distributed taken from a 20−100 ns trajectory of simulation 2 (see Table 1). The rectangular grid with a 0.5 Å resolution includes one of the *Hs*GS pentamer active sites, and an ammonium molecule was used as a probe. This methodology is frequently used to study such processes and was successfully employed previously by our group.[40−44]

QM/MM Strategy. With the aim of determining the free energy profile for the reaction catalyzed by *Hs*GS, we used MSMD combined with a QM/MM scheme. The MSMD method[45,46] was successfully used previously by our group[43,45,47−49] and comprises the use of a set of non-equilibrium pulling trajectories to obtain equilibrium properties like the free energy profile (ΔG). Briefly, in each trajectory, the system is conducted through a reaction coordinate (RC) by applying a time-dependent potential (eq 1). In our system, the RC is given by interatomic distances describing the rupture formation of bonds involved in each step of the reaction catalyzed by the enzyme.

DOI: 10.1021/acs.biochem.6b00822
Biochemistry 2016, 55, 5907−5916

$$V(t) = (1/2)k[x - x_0(t)]^2 \quad (1)$$

where k is an arbitrary constant, x is the actual RC, and x_0 is the time-dependent restraint that states the equilibrium position for the RC. The external work (W) can be computed form the force performed to drive the system and is related to ΔG by an equation known as Jarzynski's relationship:[46]

$$e^{-(\Delta G/k_B T)} = \left\langle e^{-(W/k_B T)} \right\rangle \quad (2)$$

where k_B is the Boltzmann constant and T is the temperature of the system. The brackets imply an average of several irreversible W values obtained from different trajectories. Then, to obtain an accurate ΔG profile, multiple simulations are required for the same RC, wherein different W profiles are procured by using diverse initial configurations.

As a starting point for each steering QM/MM simulation, equilibrated snapshots were randomly taken with a separation between frames of no less than 50 ps, beginning after the first 40 ns of the corresponding MD simulations described above. The procedure involves an initial optimization of 400 cycles, with subsequent thermalization to 300 K for 10 ps. The production runs were conducted over 30 ps (0.09 Å ps^{-1} of pulling velocity), with a time step of 1 fs and periodic boundary conditions.

QM System. For the analysis of the first step of the reaction, the QM system (depicted in Figure S7) includes an ATP molecule from the C5′ atom of the ribose moiety to the γ-phosphate, the three Mn^{2+} ions, two water molecules implicated in Mn^{2+} coordination, the glutamate side chain (from the β-carbon), and side chains of all protein residues that participate in Mn^{2+} coordination starting from its β-carbons (E134, E136, E196, E203, H253, and E338). The reaction coordinate comprises the breakage of the Pγ−O2G bond in the ATP molecule, and formation of a bond between the OE1 atom of the glutamate and the Pγ atom of the γ-phosphate from ATP.

$$\lambda(r) = d(\mathrm{O2G_{ATP}}{-}\mathrm{P}\gamma_{\mathrm{ATP}}) - d(\mathrm{P}\gamma_{\mathrm{ATP}}{-}\mathrm{OE1_{glu}})$$

In the case of the second step of the reaction, the QM system is almost the same (Figure S7), with the exception that the γ-phosphate belongs to the intermediate γ-glutamyl phosphate, ADP replaces ATP, and now we have an NH_3 molecule. A second QM system was studied for the second step of the reaction, in which side chains of E305 and D62′ were included. The reaction coordinate is described by the breakage of the bond of the δ-carbon of γ-Glu-P with OE1 and the formation of a bond between the N atom of ammonia and the δ-carbon of γ-Glu-P.

$$\lambda(r) = d(\mathrm{OE1_{\gamma\text{-Glu-P}}}{-}\mathrm{C}\delta_{\gamma\text{-Glu-P}}) - d(\mathrm{C}\delta_{\gamma\text{-Glu-P}}{-}\mathrm{OE1_{NH_3}})$$

QM systems have 55−65 heavy atoms (98−123 if all hydrogen atoms are included); thus, the self-consistent charge density functional tight binding (SCC-DFTB) level of theory was used to reduce the computational cost.[48] For each ΔG profile, at least 30 individual trajectories were used.

RESULTS AND DISCUSSION

***Hs*GS Structure Analysis.** The oligomeric state of *Hs*GS that is biologically relevant is a decamer, which represents a large system to be assessed by MD. Simulations of a pentamer and a dimer composed by two adjacent subunits of the pentamer were conducted to compare its performance. The system formed by the pentamer increases the computational cost by ∼30% but improves the statistical significance by 5-fold when compared with that of the dimer, making the pentamer the best option for MD regarding its cost−benefit relationship. It is worth mentioning that in mammals and plants the interactions between the pentameric rings are minor, with the loop ranging from residue 150 to 156 (human enzyme numbering) of each subunit implicated,[9] and most likely without a major impact on the active site dynamics on the time scale analyzed in this study. Therefore, all the simulations were conducted with the pentamer of *Hs*GS.

It was reported in previous crystallographic studies that when the Glu binding site is occupied by the phosphorylated form of the inhibitor L-methionine-*S*-sulfoximine (MSO-P), E305 shares a proton with D62′ and plays a very important role in the stabilization of the 302−305 loop ("E305 flap" loop[9,50]). Consistent with this, using the crystal structure of *Hs*GS complexed with manganese, ADP, and MSO-P to perform a preliminary estimation of protein residues, pK_a values revealed that a substantial population of E305 could be protonated (E305 pK_a ∼ 7.8 on average). Consequently, 100 ns MD simulations were performed for both situations, E305 protonated and deprotonated, and for the enzyme with ATP and glutamate (reactants for the first catalytic step), and with ADP, γ-Glu-P, and NH_3 or NH_4^+ (possible reactants for the second catalytic step). In all the situations considered in this work, glutamate is bound to the protein; hence, the crystal structure used to set up the systems was that corresponding to *Hs*GS with manganese, ADP, and MSO-P (for details, see Methods), also outlined earlier by other authors as the best mimicking structure that accounts for the transition state of the second step of the reaction.[50] A seventh system was included in the study comprising Mn^{2+}, ADP, NH_3, and γ-Glu-P protonated in the phosphate moiety (the explanation is discussed below). In Table 1, a list of MD simulations performed in this work is shown.

Control of the general structure stability for all systems was assessed by the root-mean-square deviation (rmsd) over protein backbone atoms, which provides a measurement of the deviation of the atoms from their original positions (Figure S1A−G), and by the root-mean-square fluctuation (rmsf) that represents the average over time of the rmsd. In Figure 2, the

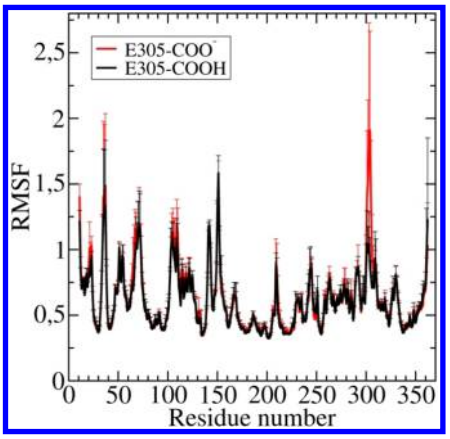

Figure 2. Backbone atom rmsf per residue for 100 ns trajectories of *Hs*GS with ATP, Mn^{2+}, and glutamate, in which E305 is protonated (black line, simulation 2 in Table 1) or deprotonated (red line, simulation 1 in Table 1). Every residue rmsf represents the mean of the five values corresponding to each subunit, and the error bars are the standard deviation.

DOI: 10.1021/acs.biochem.6b00822
Biochemistry 2016, 55, 5907−5916

per residue rmsf values for backbone atoms in simulations 1 (red line) and 2 (black line) are shown. The only noteworthy difference found between these systems encompasses residues 301−307, showing larger structural displacements when E305 is deprotonated. Furthermore, those systems with E305 deprotonated in the presence of NH_3 or NH_4^+ (simulation 3 or 5, respectively) showed higher mobility on the E305 flap loop than on the respective ones with E305 protonated [simulations 4, 6, and 7 (Figure S2)]. Therefore, the protonation state of E305 seems to be very important for maintaining the fully closed conformation of the E305 flap loop once glutamate binds to the enzyme, aided by a tight hydrogen bond interaction with D62′ carboxylate. Analysis of the distance from the E305 δ-carbon atom to the D62′ γ-carbon atom highlights how the presence of a hydrogen bond between these residues directly impacts the E305 flap loop mobility (Figure S3). The same behavior was observed upon comparison of simulations 5 with 6 and 3 with 4 and 7 (Figures S2 and S3).

It is generally accepted that the conservation of E305 (human enzyme numbering) among all species is due to its relevance in ammonium binding and deprotonation,[9,50] although these results expose the requirement of E305 as a key component in the enzyme structural features. Furthermore, the data presented here disclose the outcome of protein residue acid−base equilibrium dynamics on the conformations that the enzyme is able to visit and emphasize the importance of taking this into account when setting up the systems to perform classical MD.

Reaction Mechanism. For the generation of glutamine by condensation of ammonia with glutamate, GS must first activate glutamate by transferring a phosphate group from ATP to the side-chain carboxyl group. The second step involves the nucleophilic attack by ammonia on the δ-carbon atom of the γ-glutamyl phosphate intermediate, to finally yield the reaction products glutamine, ADP, and inorganic phosphate (Scheme 1). All phosphates participate in the coordination of Mn^{2+} (Figure 1D), and protein residues involved in the coordination are conserved among all known structures.[50] This implies that for a fully active enzyme, having all three Mn^{2+} sites occupied should be very important. Therefore, it is worth mentioning that every model system analyzed was generated with all three Mn^{2+} ions in each active site without any methodological issues, in opposition to what was previously reported,[30] where other authors excluded one Mg^{2+} ion from the active site due to clashes occurring in the preparation of the starting structures. This feature is important when studying the catalytic mechanism because of the direct participation of ATP and glutamate in metal ion coordination. In particular, the γ-phosphate from ATP that is transferred to glutamate in the first step of the reaction coordinates the three Mn^{2+} ions. Furthermore, in the complex network of coordination, the lack of any Mn^{2+} could affect the active site dynamics. The Mn^{2+} coordination microenvironment is depicted in Figure S7.

With the purpose of characterizing in detail the mechanism of both steps of the reaction catalyzed by *Hs*GS, we used MSMD simulations with a QM/MM approach to construct the reaction free energy profiles, as described in Methods. To generate the profiles, several trajectories guided through the same reaction coordinate are needed, and the starting points for each simulation were obtained from an equilibrated system of classical MD (i.e., simulations listed in Table 1). It is well-known that many enzymes have loops at or near their active sites that can adopt a different conformation upon substrate binding, turning into a "closed" state and favoring the reaction. Accordingly, for both reactions, the systems chosen to obtain the starting snapshots used to perform the MSMD were those with E305 protonated.

Additionally, to determine if the active site would be accessible to ammonia when the E305 flap loop adopts the closed conformation, the implicit ligand sampling (ILS) method was employed to determine the potential of mean force (PMF) corresponding to the placement of an ammonia molecule anywhere in the protein environment.[38,39] The result is a PMF space map that provides information about the relative probability of finding a ligand molecule in a given location, and from which an iso-energy surface is displayed. In Figure 3, ILS analysis results for closed (Figure 3A,B) and

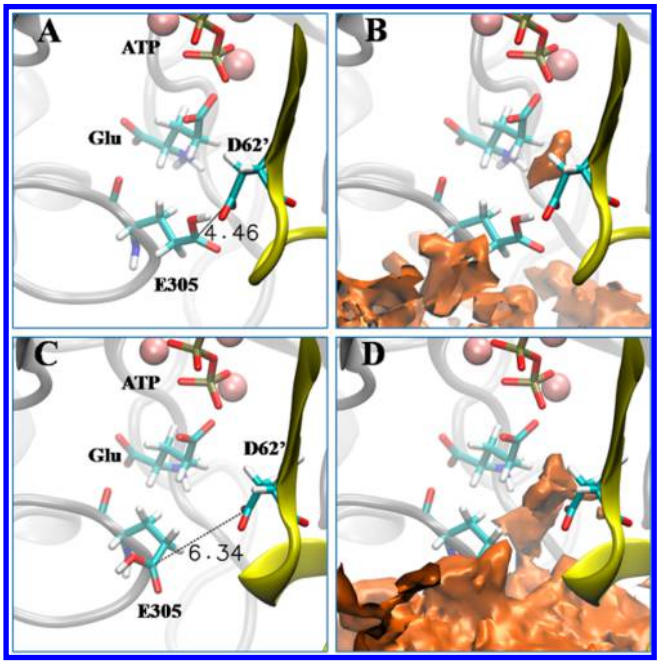

Figure 3. Evaluation of the possibility of ammonia accessing the binding site in simulation 2 by the ILS method where the E305 flap loop remains in the fully closed conformation (A and B) or in those where it is in a partially closed conformation (C and D). In the left panels, a clean picture of the active site with representative distances between E305 δ-carbon and D62′ γ-carbon atoms is displayed. In the right panels, the iso free energy surfaces obtained from PMF calculations are colored orange. ATP, Glu, E305, and D62′ are depicted in "licorice" representation, and Mn^{2+} ions are shown as pink spheres. The protein backbone is drawn as gray, with the exception of the β-sheet containing D62′, which is colored yellow.

partially closed (Figure 3C,D) conformations of *Hs*GS are shown. The volumes colored orange represent the regions where the free energy required for ammonia to occupy that place is <7 kcal/mol. Trajectory frames from simulation 2 were used for both calculations, with distances between E305 δ-carbon and D62′ γ-carbon atoms determining if it corresponds to the closed (<5 Å) or partially closed (>5 Å) conformation. Figure 3B shows a cavity near the glutamate δ-carbon atom, matching with the ammonia binding site predicted in previous studies where GS was cocrystallized with MSO-P.[9,50] The iso-energy surface in Figure 3D obtained from the PMF computed for the partially closed conformation evinces a channel connecting the bulk solution outside the protein and the ammonia binding site. This indicates that even though

DOI: 10.1021/acs.biochem.6b00822
Biochemistry 2016, 55, 5907−5916

glutamate binding promotes the closing of the E305 flap loop, a slight mobility of the loop is sufficient to allow the entrance of ammonia into the binding site. Another outcome obtained from ILS analysis is that in all considered conformations no water molecules were found to be accommodated by the ammonia binding site. This implies that hydrolysis is not likely to occur.

First Step of the Reaction: γ-Glutamyl Phosphate Formation. To address the first step of the reaction, the starting snapshots were taken from the trajectory of simulation 2 (E305 protonated), because it presented less mobility in the E305 flap loop. Via analysis of the dynamics of the MD trajectory, some fluctuations were detected in the interactions of glutamate and ATP with protein residues. Via correlation of the behavior of these interactions with the MSMD trajectories used in the free energy profile construction, it was found that the interaction of the R319 guanidinium group with the γ-phosphate and the interaction of the E136 carboxylate with the glutamate amine group had an impact on the profile outlined (Figure 4). Therefore, free energy profiles were generated by

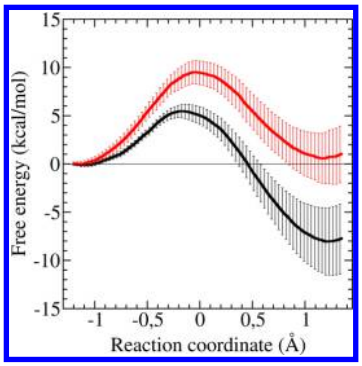

Figure 4. Free energy profiles for the first reaction, in two different conformational states, involving the direct interaction of R319 with γ-phosphate of ATP (black line), or mediated via hydrogen bonds with water molecules (red line). Error bars represent the standard deviation.

arranging the trajectories into two groups. One group includes those in which R319 accompanies the γ-phosphate along the transfer through hydrogen bonding, as well as interaction with E136 present. The second group comprises those trajectories in which either R319 is placed slightly away from the γ-phosphate with the interaction mediated by a water molecule or the glutamate amine group moves away from the E136 carboxylate.

Thereby, for the transfer of the γ-phosphate group from ATP to the side-chain carboxyl group of glutamate, an exergonic reaction with a ΔG of −8.0 kcal/mol and a small barrier of 5 kcal/mol was obtained (Figure 4, black line) when the two mentioned interactions were present. However, if any of these interactions are lost, the reaction ΔG obtained is close to zero (1 kcal/mol) and the barrier increases to 9.5 kcal/mol (Figure 4, red line). Thus, these interactions affect the reaction kinetics as well as the thermodynamics by stabilizing the transition state and the intermediate reaction product γ-Glu-P.

The influence of the E136−glutamate interaction on the free energy profile can be explained by attributing to it the proper positioning of the substrate. On the other hand, the electrostatic interaction of R319 with γ-phosphate is very important, aiding the transfer to form γ-glutamyl phosphate. From distance analysis presented in Figure S4, we can notice that the breakage of the interaction of the γ-phosphate with R319 occurs only when E305−D62′ hydrogen bonding is disrupted (i.e., E305 Cδ···Cγ D62′ distance of >5 Å), indicating a dependence on the fully closed conformation of the E305 flap loop. Distance analysis between the γ-phosphate with the R319 guanidinium group, including data from all subunits, is shown in Figure S5. These results imply that the first reaction becomes more favored to occur in those conformations in which E305 interacts by hydrogen bonding with D62′. Finally, if in the fully closed conformation of the E305 flap loop E305 and D62′ are interacting by hydrogen bonding with each other, it seems unlikely that any of these residues would be responsible for deprotonation of ammonium as proposed above, even though these residues are directly interacting with ammonium (Figure 5B[50]). The phosphate transfer is also represented as a three-dimensional (3D) animation (see the Supporting Information).

Second Step of the Reaction: Ammonia Nucleophilic Attack. In the same way that was used for the first reaction, 100 ns MD trajectories of simulations 4, 6, and 7 were used to obtain the initial snapshots for the MSMD analysis of the second step of the reaction catalyzed by *Hs*GS. The selection of the different situations arises from contemplating the possibility that the phosphate moiety of intermediate γ-Glu-P could be protonated (γ-Glu-P-H). Considering the pK_a values of inorganic phosphate in aqueous solution (∼2.2, ∼7.2, and ∼12.6), it is probable that at least the single protonated form would make it a better leaving group, even though most likely the protein environment would modify these pK_a values.

As it was proposed that E305 and D62′ are involved in ammonium deprotonation,[50] we tried to test deprotonated E305 and D62′ proton affinities in the presence of NH_4^+. Unfortunately, attempts to prepare the QM/MM system from simulation 5 were unsuccessful.

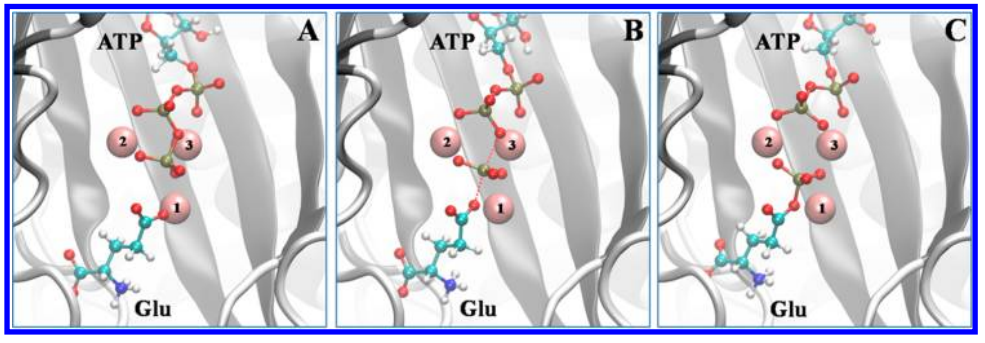

Figure 5. (A) Reactants, (B) transition state, and (C) products for the first step of the reaction catalyzed by *Hs*GS. Glu and ATP are shown in "ball and stick" representation; protein backbones are depicted as gray ribbons, and Mn^{2+} ions are shown as pink spheres (numbered as 1−3).

DOI: 10.1021/acs.biochem.6b00822
Biochemistry 2016, 55, 5907−5916

As one can see in the free energy profiles presented in Figure 6A, γ-Glu-P-H is indeed the substrate that displays the most

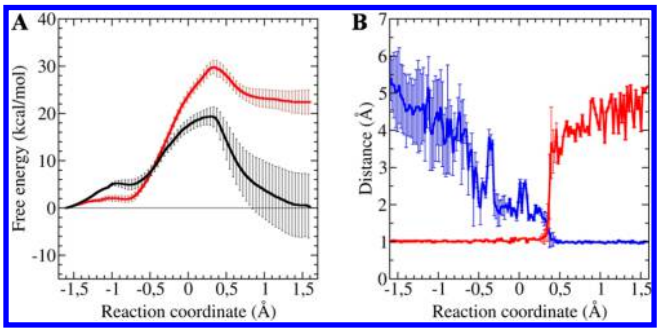

Figure 6. (A) Free energy profiles for the second step of the reaction. Error bars represent the standard deviation. The profile colored red corresponds to the reaction in which γ-Glu-P is the intermediate, whereas the black line is the profile for the reaction with γ-Glu-P-H as the reaction intermediate. (B) Distance analysis related to the proton transferred from NH_3 to E196. Distances to the NH_3 nitrogen (red line) and to the carbonyl oxygen of E196 (blue line) are illustrated. Error bars represent the standard deviation.

thermodynamically favorable conditions (black line), decreasing the reaction Δ*G* from 22 kcal/mol to almost zero when compared with that with γ-Glu-P as an intermediate and NH_3 as a nucleophile (Figure 6A, red line). In addition, a decrease in the activation Δ*G* from 29 to 19 kcal/mol is observed. Although a large decrease in the product free energy was found when γ-Glu-P-H was studied as a reaction intermediate, it should be noted that this calculation lacks a possible final stabilization due to the release of the products from the active site. In the system composed by γ-Glu-P-H, during the nucleophilic attack a proton from NH_3 is taken by the E196 carboxylate, although E305 and D62′ are included in the QM subsystem and are interacting directly with NH_3 (Figure 7A). This event was observed in all pulling trajectories corresponding to the simulation 7 starting snapshots (Figure 6A, black line), indicating that in this QM system E196 might be the best candidate to act as a "proton relay". The bond breaking and formation involved in the mechanism proceed in a symmetric manner (Figure 6B). The hydrogen bond between ammonia and the E196 carboxyl group accompanies the transition state, and finally, the proton transfer from NH_3 to E196 indicates the end of the transition state marking the progress of the reaction coordinate toward the products (Figure 6B). Mean values were obtained by weighting each value by the contribution of the corresponding work to the free energy calculation. Representative snapshots of structures of reactants, the transition state, and products for this reaction step are depicted in Figure 7A–C.

When the free energy profile obtained for the first step of the reaction is taken into account (Figure 4), it seems like the second step could be limiting the reaction kinetics. This result is consistent with that obtained recently by other authors.[31] The K_M values of *Hs*GS for glutamate and ammonia reported by Listrom et al.[51] are 3 and 0.16 mM, respectively. Interestingly, the average concentration of glutamate in human brain is around 10–12 mM, being highly regulated between the extracellular fluid (0.5–5 μM) and nerve cell cytosol, and in synaptosomal vesicles can be higher than 100 mM.[52] This implies that GS will be saturated with glutamate. On the other hand, the ammonia brain concentration is ∼0.18 mM,[52] quite similar to the K_M of 0.16 mM reported by Listrom et al.[51] All these findings together suggest that GS activity will be highly sensitive to changes in ammonium concentration, with glutamate acting as a buffer.[52]

With respect to the protonation state of γ-glutamyl phosphate and the need for NH_4^+ to lose a proton to become a nucleophile, it is possible that the phosphate group from γ-Glu-P could take that proton from ammonium, producing an ammonia molecule suitably positioned for nucleophilic attack. Similar to what was observed with simulation 7 as a starting point (Figure 6A, black line), MSMD performed with snapshots taken from simulation 6 showed first the transfer of a proton from NH_4^+ to the phosphate moiety of γ-Glu-P and then the transfer of a second proton from NH_3 to E196. Adversely, this system yielded an activation Δ*G* of ∼50 kcal/mol (data not shown), which is quite plausible because proton transfer processes are very important in phosphate transfer and/or hydrolysis and may be not easy to describe with these methodologies.

On the other hand, in all the pulling trajectories in which simulation 4 was used as a starting point (Figure 6A, red line), during the nucleophilic attack a hydrogen atom from NH_3 is caught by the phosphate moiety form γ-Glu-P, supporting the idea that this group is quite likely to become protonated. When γ-Glu-P-H is used as the starting reaction intermediate, a bypass of the proton transfer could probably be lowering the profile of the work done from the beginning of the pulling trajectory. In Figure S6, we depict a histogram for distances between the NH_4^+ nitrogen and an oxygen from the γ-Glu-P phosphate moiety (simulation 6), in which it can be seen that a strong hydrogen bond is present during the time scale of the simulation, and in all subunits of the pentamer. However, the

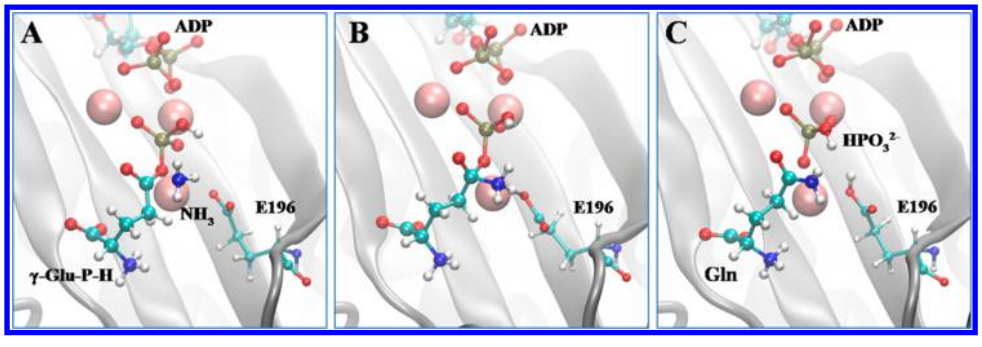

Figure 7. Representative images of the (A) reactants, (B) transition state, and (C) products taken from one QM/MM-guided trajectory corresponding to the system described by simulation 7. ADP, E196, γ-Glu-P-H, Gln, and HPO_4^{2-} are shown in "ball and stick" representation; protein backbones are depicted as gray ribbons, and Mn^{2+} ions are shown as pink spheres (numbered 1–3).

DOI: 10.1021/acs.biochem.6b00822
Biochemistry 2016, 55, 5907–5916

phosphate moiety from γ-Glu-P might also become protonated through an acid−base equilibrium with water without needing ammonium to be present. Similarly, ammonium could turn into ammonia by the same means once it has entered the active site.

It was previously proposed by other authors that D62′ would be responsible for deprotonation of ammonium to produce ammonia that will operate as a nucleophile.[50] Moreover, in a very recent publication, other authors presented a QM/MM study for the reaction mechanism of *M. tuberculosis* GS, and the protonation state of E305 and D62′ (human enzyme numbering) was not taken under consideration, setting E305 as its conjugate base.[31] In the mentioned study, the QM/MM protocol from which free energies were calculated was made using the geometrically optimized crystal structures, where the environment surrounding E305 and D62′ gives these residues a high proton affinity. As expected, the results obtained by Moreira et al. showed that D62′ deprotonates ammonium. On the other hand, our results that consider protein dynamics showed that the binding of glutamate promotes the closed conformation of the E305 flap loop, which in turn induces the interaction of E305 with D62′ by hydrogen bonding. Sharing a proton will disable both residues to take a proton from ammonium. Furthermore, the results show that the phosphate moiety could be a good candidate for deprotonation of ammonium (in the case of not being already protonated), besides making it a good leaving group. In the Supporting Information, a 3D animation of the nucleophilic attack process is presented.

CONCLUSIONS

Herein, we present a detailed analysis of *Hs*GS dynamic behavior and the chemical reactions that are involved in *Hs*GS catalytic mechanism, in terms of classical and multiscale QM/MM MD simulations together with reaction free energy profile determinations. Our results show that both steps of the mechanism can be described as bimolecular nucleophilic substitutions (S_N2), involving the transfer of a phosphate group from ATP to glutamate, activating the glutamate δ-carbon for a further nucleophilic attack by ammonia, yielding glutamine, ADP, and P_i. Furthermore, starting from the information obtained through classical MD analysis and supplemented with the MSMD results, we exposed the importance of the acid−base equilibrium underlying the catalytic mechanism of *Hs*GS.

The results presented in this study indicate that the formation of the γ-glutamyl phosphate intermediate is strongly favored by the fully closed conformation of the E305 flap loop, which is very much influenced by the E305 protonation state, that revealed a direct impact on this loop dynamics. The presence of a hydrogen bond between E305 and D62′ turned out to be essential for preserving the closed conformation of the E305 flap loop. Once the loop has adopted an open conformation, the hydrogen bond interaction of the γ-phosphate with R319 is disrupted, affecting the kinetics and thermodynamics of the phosphate transfer reaction.

The second step depends on the transfer of two protons from the nucleophile that yields the amine moiety in glutamine. First, ammonium needs to lose a proton and turn into ammonia to become a good nucleophile. In this process, the phosphate moiety of the γ-glutamyl phosphate intermediate might be involved in deprotonation of ammonium, and not D62′ as previously suggested. Regardless, the results indicate that at least a single protonation of the phosphate moiety from γ-glutamyl phosphate makes it a better leaving group, and the presence of hydrogen bonding between E305 and D62′ would prevent these residues from participating in the deprotonation of ammonium.

Finally, the analysis of the free energy profiles computed for both reactions reveals that the nucleophilic attack of ammonia represents the rate-limiting step in the formation of glutamine. These results are in good agreement with bibliographic data related to kinetic rate constants and *in vivo* ligand concentrations.

ASSOCIATED CONTENT

Supporting Information

The Supporting Information is available free of charge on the ACS Publications website at DOI: 10.1021/acs.biochem.6b00822.

General structure controls by rmsd and rmsf, a description of the QM/MM system, 3D animation specifications, and additional distance analysis supporting the results presented in the text (PDF)

Three-dimensional (3D) animation of the phosphate transfer (AVI)

Three-dimensional (3D) animation of the nucleophilic attack process (AVI)

AUTHOR INFORMATION

Corresponding Authors

*E-mail: sbartesa@fmed.edu.uy. Telephone: (5982)9249561. Fax: (5982)9249563.

*E-mail: dario@qi.fcen.uba.ar. Telephone: (5411)45763358. Fax: (5411)45763341.

Funding

F.M.I. was supported by a postdoctoral fellowship from CONICET, and N.C. was partially supported by a doctoral fellowship from Universidad de la República (CAP). This work was supported by grants from Universidad de Buenos Aires (Grant 20020130100097BA) and CONICET to D.A.E., Agencia Nacional de Investigación e Innovación to S.B. (FCE_2001_2_6605, ANII, Uruguay), Universidad de la República to R.R. (CSIC and EI), and Alexander Von Humboldt Foundation to T.G and R.R. Additional support was obtained from the Centro de Biologia Estructural del Mercosur (CeBEM).

Notes

The authors declare no competing financial interest.

ACKNOWLEDGMENTS

The authors thank Centro de Cómputos de Alto Rendimiento (CeCAR) and Cristina cluster from Centro de Computación de Alto Desempeño (CCAD, Universidad Nacional de Córdoba) for allowing use of computational resources that allowed us to perform part of the experiments included in this work.

ABBREVIATIONS

GS, glutamine synthetase; *Hs*GS, human glutamine synthetase; Glu, glutamate; γ-Glu-P, γ-glutamyl phosphate; γ-Glu-P-H, monoprotonated γ-glutamyl phosphate; MD, molecular dynamics; MM, molecular mechanics; QM, quantum mechanics; MSO-P, L-methionine-*S*-sulfoximine phosphate; P_i, inorganic phosphate; rmsd, root-mean-square deviation; rmsf,

DOI: 10.1021/acs.biochem.6b00822
Biochemistry 2016, 55, 5907−5916

root-mean-square fluctuation; VMD, Visual Molecular Dynamics.

REFERENCES

(1) van Rooyen, J. M., Abratt, V. R., Belrhali, H., and Sewell, T. (2011) Crystal structure of type III glutamine synthetase: Surprising reversal of the inter-ring interface. *Structure 19*, 471−483.

(2) Pesole, G., Bozzetti, M., Lanave, C., Preparata, G., and Saccone, C. (1991) Glutamine synthetase gene evolution: a good molecular clock. *Proc. Natl. Acad. Sci. U. S. A. 88*, 522−526.

(3) Kumada, Y., Benson, D., Hillemann, D., Hosted, T., Rochefort, D., Thompson, C., Wohlleben, W., and Tateno, Y. (1993) Evolution of the glutamine synthetase gene, one of the oldest existing and functioning genes. *Proc. Natl. Acad. Sci. U. S. A. 90*, 3009−3013.

(4) Bernard, S. M., and Habash, D. Z. (2009) The importance of cytosolic glutamine synthetase in nitrogen assimilation and recycling. *New Phytol. 182*, 608−620.

(5) Mathis, R., Gamas, P., Meyer, Y., and Cullimore, J. V. (2000) The presence of GSI-like genes in higher plants: support for the paralogous evolution of GSI and GSII genes. *J. Mol. Evol. 50*, 116−122.

(6) Wistow, G., Bernstein, S. L., Wyatt, M. K., Behal, A., Touchman, J. W., Bouffard, G., Smith, D., and Peterson, K. (2002) Expressed sequence tag analysis of adult human lens for the NEIBank Project: over 2000 non-redundant transcripts, novel genes and splice variants. *Mol. Vision 8*, 171−184.

(7) Wyatt, K., White, H. E., Wang, L., Bateman, O. A., Slingsby, C., Orlova, E. V., and Wistow, G. (2006) Lengsin is a survivor of an ancient family of class I glutamine synthetases re-engineered by evolution for a role in the vertebrate lens. *Structure 14*, 1823−1834.

(8) Unno, H., Uchida, T., Sugawara, H., Kurisu, G., Sugiyama, T., Yamaya, T., Sakakibara, H., Hase, T., and Kusunoki, M. (2006) Atomic Structure of Plant Glutamine Synthetase: A Key Enzyme For Plant Productivity. *J. Biol. Chem. 281*, 29287−29296.

(9) Krajewski, W. W., Collins, R., Holmberg-Schiavone, L., Jones, T. A., Karlberg, T., and Mowbray, S. L. (2008) Crystal structures of mammalian glutamine synthetases illustrate substrate-induced conformational changes and provide opportunities for drug and herbicide design. *J. Mol. Biol. 375*, 217−228.

(10) Yamashita, M., Almassy, R., Janson, C., Cascio, D., and Eisenberg, D. (1989) Refined atomic model of glutamine synthetase at 3.5 A resolution. *J. Biol. Chem. 264*, 17681−17690.

(11) Eisenberg, D., Gill, H. S., Pfluegl, G. M., and Rotstein, S. H. (2000) Structure−function relationships of glutamine synthetases. *Biochim. Biophys. Acta, Protein Struct. Mol. Enzymol. 1477*, 122−145.

(12) Ginsburg, A. (1972) Glutamine synthetase of Escherichia coli: some physical and chemical properties. *Adv. Protein Chem. 26*, 1−79.

(13) Melo, P. M., Silva, L. S., Ribeiro, I., Seabra, A. R., and Carvalho, H. G. (2011) Glutamine synthetase is a molecular target of nitric oxide in root nodules of Medicago truncatula and is regulated by tyrosine nitration. *Plant Physiol. 157*, 1505−1517.

(14) De Pinto, V., Caggese, C., Prezioso, G., and Ritossa, F. (1987) Purification of the glutamine synthetase II isozyme of Drosophila melanogaster and structural and functional comparison of glutamine synthetases I and II. *Biochem. Genet. 25*, 821−836.

(15) Matthews, G. D., Gould, R. M., and Vardimon, L. (2005) A single glutamine synthetase gene produces tissue-specific subcellular localization by alternative splicing. *FEBS Lett. 579*, 5527−5534.

(16) Popoli, M., Yan, Z., McEwen, B. S., and Sanacora, G. (2012) The stressed synapse: the impact of stress and glucocorticoids on glutamate transmission. *Nat. Rev. Neurosci. 13*, 22−37.

(17) Qvartskhava, N., Lang, P. A., Görg, B., Pozdeev, V. I., Ortiz, M. P., Lang, K. S., Bidmon, H. J., Lang, E., Leibrock, C. B., Herebian, D., Bode, J. G., Lang, F., and Häussinger, D. (2015) Hyperammonemia in gene-targeted mice lacking functional hepatic glutamine synthetase. *Proc. Natl. Acad. Sci. U. S. A. 112*, 5521−5526.

(18) Suarez, I., Bodega, G., and Fernandez, B. (2002) Glutamine synthetase in brain: effect of ammonia. *Neurochem. Int. 41*, 123−142.

(19) Robinson, S. R. (2000) Neuronal expression of glutamine synthetase in Alzheimer's disease indicates a profound impairment of metabolic interactions with astrocytes. *Neurochem. Int. 36*, 471−482.

(20) Kulijewicz-Nawrot, M., Syková, E., Chvátal, A., Verkhratsky, A., and Rodríguez, J. J. (2013) Astrocytes and glutamate homoeostasis in Alzheimer's disease: a decrease in glutamine synthetase, but not in glutamate transporter-1, in the prefrontal cortex. *ASN Neuro 5*, 273−282.

(21) Robinson, S. R. (2001) Changes in the cellular distribution of glutamine synthetase in Alzheimer's disease. *J. Neurosci. Res. 66*, 972−980.

(22) Olabarria, M., Noristani, H. N., Verkhratsky, A., and Rodríguez, J. J. (2011) Age-dependent decrease in glutamine synthetase expression in the hippocampal astroglia of the triple transgenic Alzheimer's disease mouse model: mechanism for deficient glutamatergic transmission? *Mol. Neurodegener. 6*, 55.

(23) Souza, D. G., Bellaver, B., Raupp, G. S., Souza, D. O., and Quincozes-Santos, A. (2015) Astrocytes from adult Wistar rats aged in vitro show changes in glial functions. *Neurochem. Int. 90*, 93−97.

(24) Häberle, J., Görg, B., Rutsch, F., Schmidt, E., Toutain, A., Benoist, J.-F., Gelot, A., Suc, A.-L., Höhne, W., Schliess, F., Häussinger, D., and Koch, H. G. (2005) Congenital glutamine deficiency with glutamine synthetase mutations. *N. Engl. J. Med. 353*, 1926−1933.

(25) Häberle, J., Görg, B., Toutain, A., Rutsch, F., Benoist, J.-F., Gelot, A., Suc, A.-L., Koch, H. G., Schliess, F., and Häussinger, D. (2006) Inborn error of amino acid synthesis: human glutamine synthetase deficiency. *J. Inherited Metab. Dis. 29*, 352−358.

(26) Krishnaswamy, P., Pamiljans, V., and Meister, A. (1960) Activated glutamate intermediate in the enzymatic synthesis of glutamine. *J. Biol. Chem. 235*, PC39−PC40.

(27) Wedler, F., and Boyer, P. (1972) Substrate binding and reaction intermediates of glutamine synthetase (Escherichia coli W) as studied by isotope exchanges. *J. Biol. Chem. 247*, 984−992.

(28) Wedler, F. C., and Horn, B. R. (1976) Catalytic mechanisms of glutamine synthetase enzymes. Studies with analogs of possible intermediates and transition states. *J. Biol. Chem. 251*, 7530−7538.

(29) Liaw, S. H., and Eisenberg, D. (1994) Structural model for the reaction mechanism of glutamine synthetase, based on five crystal structures of enzyme-substrate complexes. *Biochemistry 33*, 675−681.

(30) Frieg, B., Görg, B., Homeyer, N., Keitel, V., Häussinger, D., and Gohlke, H. (2016) Molecular Mechanisms of Glutamine Synthetase Mutations that Lead to Clinically Relevant Pathologies. *PLoS Comput. Biol. 12*, e1004693.

(31) Moreira, C., Ramos, M. J., and Fernandes, P. A. (2016) Reaction Mechanism of Mycobacterium Tuberculosis Glutamine Synthetase Using Quantum Mechanics/Molecular Mechanics Calculations. *Chem. - Eur. J. 22*, 9218−9225.

(32) Dolinsky, T. J., Czodrowski, P., Li, H., Nielsen, J. E., Jensen, J. H., Klebe, G., and Baker, N. A. (2007) PDB2PQR: expanding and upgrading automated preparation of biomolecular structures for molecular simulations. *Nucleic Acids Res. 35*, W522−W525.

(33) Humphrey, W., Dalke, A., and Schulten, K. (1996) VMD: visual molecular dynamics. *J. Mol. Graphics 14*, 33−38.

(34) Bayly, C. I., Cieplak, P., Cornell, W., and Kollman, P. A. (1993) A well-behaved electrostatic potential based method using charge restraints for deriving atomic charges: the RESP model. *J. Phys. Chem. 97*, 10269−10280.

(35) Meagher, K. L., Redman, L. T., and Carlson, H. A. (2003) Development of polyphosphate parameters for use with the AMBER force field. *J. Comput. Chem. 24*, 1016−1025.

(36) Essmann, U., Perera, L., Berkowitz, M. L., Darden, T., Lee, H., and Pedersen, L. G. (1995) A smooth particle mesh Ewald method. *J. Chem. Phys. 103*, 8577−8593.

(37) Ryckaert, J.-P., Ciccotti, G., and Berendsen, H. J. (1977) Numerical integration of the cartesian equations of motion of a system with constraints: molecular dynamics of n-alkanes. *J. Comput. Phys. 23*, 327−341.

DOI: 10.1021/acs.biochem.6b00822
Biochemistry 2016, 55, 5907−5916

(38) Cohen, J., Arkhipov, A., Braun, R., and Schulten, K. (2006) Imaging the migration pathways for O 2, CO, NO, and Xe inside myoglobin. *Biophys. J. 91*, 1844−1857.
(39) Cohen, J., Olsen, K. W., and Schulten, K. (2008) Finding gas migration pathways in proteins using implicit ligand sampling. *Methods Enzymol. 437*, 439−457.
(40) Boron, I., Capece, L., Pennacchietti, F., Wetzler, D. E., Bruno, S., Abbruzzetti, S., Chisari, L., Luque, F. J., Viappiani, C., Marti, M. A., Estrin, D. A., and Nadra, A. D. (2015) Engineered chimeras reveal the structural basis of hexacoordination in globins: A case study of neuroglobin and myoglobin. *Biochim. Biophys. Acta, Gen. Subj. 1850*, 169−177.
(41) Bustamante, J. P., Abbruzzetti, S., Marcelli, A., Gauto, D., Boechi, L., Bonamore, A., Boffi, A., Bruno, S., Feis, A., Foggi, P., Estrin, D. A., and Viappiani, C. (2014) Ligand uptake modulation by internal water molecules and hydrophobic cavities in hemoglobins. *J. Phys. Chem. B 118*, 1234−1245.
(42) Bustamante, J. P., Radusky, L., Boechi, L., Estrin, D. A., ten Have, A., and Martí, M. A. (2016) Evolutionary and functional relationships in the truncated hemoglobin family. *PLoS Comput. Biol. 12*, e1004701.
(43) Forti, F., Boechi, L., Estrin, D. A., and Marti, M. A. (2011) Comparing and combining implicit ligand sampling with multiple steered molecular dynamics to study ligand migration processes in heme proteins. *J. Comput. Chem. 32*, 2219−2231.
(44) Marcelli, A., Abbruzzetti, S., Bustamante, J. P., Feis, A., Bonamore, A., Boffi, A., Gellini, C., Salvi, P. R., Estrin, D. A., Bruno, S., Viappiani, C., and Foggi, P. (2012) Following ligand migration pathways from picoseconds to milliseconds in type II truncated hemoglobin from Thermobifida fusca. *PLoS One 7*, e39884.
(45) Crespo, A., Martí, M. A., Estrin, D. A., and Roitberg, A. E. (2005) Multiple-steering QM-MM calculation of the free energy profile in chorismate mutase. *J. Am. Chem. Soc. 127*, 6940−6941.
(46) Jarzynski, C. (1997) Nonequilibrium equality for free energy differences. *Phys. Rev. Lett. 78*, 2690.
(47) Capece, L., Estrin, D. A., and Marti, M. A. (2008) Dynamical characterization of the heme NO oxygen binding (HNOX) domain. Insight into soluble guanylate cyclase allosteric transition†. *Biochemistry 47*, 9416−9427.
(48) Defelipe, L. A., Lanzarotti, E., Gauto, D., Marti, M. A., and Turjanski, A. G. (2015) Protein topology determines cysteine oxidation fate: the case of sulfenyl amide formation among protein families. *PLoS Comput. Biol. 11*, e1004051.
(49) Xiong, H., Crespo, A., Marti, M., Estrin, D., and Roitberg, A. E. (2006) Free energy calculations with non-equilibrium methods: applications of the Jarzynski relationship. *Theor. Chem. Acc. 116*, 338−346.
(50) Krajewski, W. W., Jones, T. A., and Mowbray, S. L. (2005) Structure of Mycobacterium tuberculosis glutamine synthetase in complex with a transition-state mimic provides functional insights. *Proc. Natl. Acad. Sci. U. S. A. 102*, 10499−10504.
(51) Listrom, D. C., Morizono, H., Rajagopal, S. B., McCann, T. M., Tuchman, M., and Allewell, M. N. (1997) Expression, purification, and characterization of recombinant human glutamine synthetase. *Biochem. J. 328*, 159−163.
(52) Cooper, A. J., and Jeitner, T. M. (2016) Central Role of Glutamate Metabolism in the Maintenance of Nitrogen Homeostasis in Normal and Hyperammonemic Brain. *Biomolecules 6*, 16.

DOI: 10.1021/acs.biochem.6b00822
Biochemistry 2016, 55, 5907−5916